Nano Research 2018, 11(6): 3096–3105
https://doi.org/10.1007/s12274-017-1716-y
Research Article
ISSN 1998-0124
CN 11-5974/O4

Au nanocomposite enhanced electret film for triboelectric nanogenerator

Bao Dong Chen[1,2,§], Wei Tang[1,2,§], Chi Zhang[1,2,§], Liang Xu[1,2], Lai Pan Zhu[1,2], Lei Jing Yang[1,2], Chuan He[1,2], Jian Chen[1,2], Long Liu[1,2], Tao Zhou[1,2], and Zhong Lin Wang[1,2,3] (✉)

[1] *Beijing Institute of Nanoenergy and Nanosystems, Chinese Academy of Sciences, Beijing 100083, China*
[2] *CAS Center for Excellence in Nanoscience, National Center for Nanoscience and Technology (NCNST), Beijing 100190, China*
[3] *School of Material Science and Engineering, Georgia Institute of Technology, Atlanta, Georgia 30332, USA*
[§] *Bao Dong Chen, Wei Tang and Chi Zhang contributed equally to this work.*

Received: 9 April 2017
Revised: 23 May 2017
Accepted: 10 June 2017

KEYWORDS
equivalent nanocapacitor structure, polytetrafluoroethylene (PTFE) electret thin film, gold nanoparticles, equivalent surface charge density

ABSTRACT

A triboelectric nanogenerator (TENG) with an organic nanocomposite electret thin film as the triboelectric layer for mechanical energy harvesting was investigated systematically. In combination with corona charging, a TENG was fabricated by using embedded-nanocapacitor-structure polytetrafluoroethylene (PTFE) impregnated with gold nanoparticles (Au-NPs). The output performances, stability, and durability of the TENGs with Au-PTFE nanocomposite films were characterized after being washed in water. It was found that the output current increases by 70% and the equivalent surface charge density (ESCD) reaches 85 μC/m² in comparison to the virgin PTFE film. Such outstanding performance is likely due to the equivalent nanocapacitors between the Au-NPs and PTFE molecules, which serve as nano charge traps in the nanocomposite electret film under negative high-voltage corona charging. This work not only expands the practical applications of TENGs, but also opens up new possibilities for the development of high performance triboelectric materials.

1 Introduction

In the past four years, triboelectric nanogenerators (TENGs) based on triboelectrification and electrostatic induction have been extensively investigated [1–7]. This new technology can effectively convert arbitrary vibrational energy from the ambient environment, including body movement [8–10], water waves [11–13], wing motion [14] and other mechanical energy into electricity [15–17]. Recently, TENGs have been applied to run low-power electronics [18–20], self-powered sensors [21–23] and remove $PM_{2.5}$ particles in air purification systems [24]. TENGs have been demonstrated to have the potential to provide sustainable power sources for portable electronics.

Organic electret film is widely used in micro-

Address correspondence to zlwang@gatech.edu

electro-mechanical systems, sensors and many other fields due to its excellent negative voltage capacity and superior stored charge density [25, 26]. Since the output performance of the TENGs is proportional to the equivalent surface charge density (ESCD) on the triboelectric layers, the use of an organic electret film as the tribo-material has been suggested for the enhancement of output [27–29]. Among them, polytetrafluoroethylene (PTFE) is a promising electret and has been widely investigated for its use in TENGs, owing to its high charge storage capability and stability [30–32]. In combination with the corona charging method [33, 34], we designed an embedded-nanocapacitor-structure PTFE through filling with gold nanoparticles (Au-NPs). The microstructure and surface potential distribution of the Au-PTFE nanocomposite films with different Au-NP concentrations were characterized. The output performances, stability, and durability of the TENGs based on the Au-PTFE nanocomposite films after being washed in water were investigated. Furthermore, the enhancement mechanism of the nanocapacitor structure is discussed in detail.

2 Experimental

Au-PTFE nanocomposite films were prepared by filling pure PTFE with Au-NP dispersions; Fig. 1(a) shows the fabrication process in detail. In this experiment, the pure PTFE aqueous emulsion (Teflon DISP40, DuPont) contained both the solid granule and the liquid dispersant at the weight ratio of 3:2, and Au-NP dispersion concentration was approximately 700 parts per million (ppm). To fabricate Au-PTFE nanocomposite film, the PTFE aqueous emulsion was placed in a graduated cylinder (20 mL), and then different volumes of the Au-NP dispersion were added. The mixture was quickly stirred with a magnetic stirrer for 20 min to disperse the Au-NPs uniformly in the

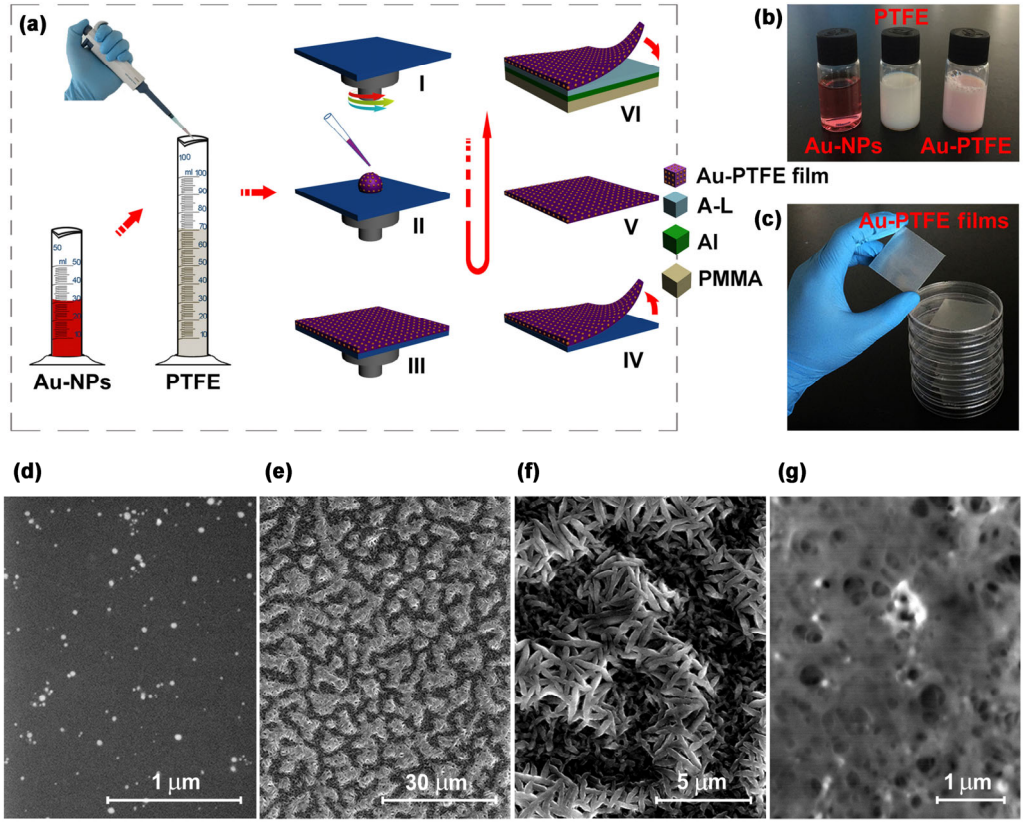

Figure 1 Schematic diagrams of the process for fabricating the Au-PTFE nanocomposite thin film and its micro-morphology. (a) Schematic diagrams of the process for preparing the Au-PTFE nanocomposite films by spin-coating. (b) Digital image of the Au NPs aqueous dispersion, pure PTFE aqueous dispersion and hybrid aqueous dispersion of the two. (c) Digital image of the Au-PTFE nanocomposite films. (d) SEM images of the Au-NPs. (e)–(g) SEM images of the Au-PTFE nanocomposite film under different magnifications.

PTFE aqueous emulsion. Figure 1(b) shows a digital image of the Au-NP dispersion, the pure PTFE aqueous emulsion and Au-PTFE hybrid aqueous dispersion. Then, a low-cost, non-vacuum spin-coating process was used to prepare the Au-PTFE nanocomposite films on a square aluminum substrate with dimensions of 5 cm × 5 cm × 0.2 mm. Figure 1(c) shows the synthesized Au-PTFE nanocomposite films. Finally, the Au-PTFE nanocomposite film was peeled off the aluminum substrate. Scanning electron microscopy (SEM) images of the Au-PTFE nanocomposite films' morphology and microstructure are shown in Figs. 1(d)–1(g). Self-assembled corona charging equipment was used to charge the Au-PTFE nanocomposite film. The distribution characteristics of the surface potential on the Au-PTFE nanocomposite film was then measured using atomic force microscopy (AFM).

Subsequently, we utilized the Au-PTFE nanocomposite films to construct a contact-separation mode TENG, where one part was comprised of an Au-PTFE nanocomposite film (5 μm), an adhesion-layer (A-L), an aluminum foil (Al, 100 mm), and the substrate of polymethylmethacrylic (PMMA, 3 mm). The Au-PTFE nanocomposite film serves as the tribo-material, and the aluminum foil serves as the electrode connected with the external load. The TENG's counterpart is an aluminum electrode, which is utilized to make contact with the Au-PTFE film. The liquid water used was deionized for the stability and durability test of TENG's output electricity. A linear motor was used to control the displacement, frequency, and to produce uniform contact. The output signals of the TENG based on Au-PTFE nanocomposite film were measured by a Keithley voltage preamplifier and a data acquisition card.

3 Results and discussion

Figures 1(d)–1(g) show SEM images of Au-NPs and the Au-PTFE nanocomposite film. The Au-NP sizes were about 10 to 30 nm, were well dispersed, and the PTFE film was homogeneous. From Fig. 1(g) we can clearly see the Au-NPs distributed uniformly in the PTFE film. The experimental apparatus used for corona charging is shown in Fig. 2(a). The aluminum foil electrode was adhered to the back of the Au-PTFE nanocomposite film and the pin electrode was placed above the film with a vertical distance of 5 cm. By applying a high negative voltage of –5 kV across the pin electrode and the aluminum foil electrode for 5 min, the air between them was broken down and ionized, and the as-produced electrons and negative ions were injected into the Au-PTFE nanocomposite film under the electric field [25, 31]. To investigate the role of Au-NPs in improving the ESCD of PTFE electret film, Au-NPs with different volumes (0–5.00 mL, 700 ppm) were filled into PTFE aqueous emulsion to form films with identical dimensions of 4 cm × 4 cm × 5 μm. The surface potentials of the Au-PTFE nanocomposite films were monitored over time, and are shown in Fig. 2(b). They all show a similar nonlinear attenuation trend with the increase of exposure time, and gradually reached stability after 20 min (Fig. 2(c)). However, the stable surface potential increased with the increase of Au-NP volume, and reached its maximum value at 0.50 mL. Specifically, the stable potential increases from –88 V (without Au-NPs) to –229 V (with 0.50 mL of 700 ppm Au-NPs). The output began to drop with further increase in Au-NP concentration. To further analyze the storage stability of charge injection, the surface potentials of the Au-PTFE nanocomposite films with different Au-NP concentrations were measured after being immersed in deionized water for 5 min (Fig. 2(d)). The Au-PTFE nanocomposite film with 0.50 mL of Au-NPs gave the maximum charge storage. Therefore, through the Au-NP doping method, both the charge density and storage ability of the Au-PTFE nanocomposite film after corona charge were enhanced. To investigate the effect of the Au-NPs embedded in PTFE film on the output performance of the TENG, the Au-PTFE nanocomposite films were utilized to construct a contact-separation mode TENG, with a contact area of 4 cm × 4 cm. Each nanocomposite film after corona charging was exposed to air for 30 min. The open-circuit voltage, short-circuit current and transferred charge quantity of the TENGs were measured under a fixed contact frequency and force via a linear motor, as shown in Fig. 3(a). The working mechanism of the TENG is illustrated in Fig. 3(b). Both the open-circuit voltage and short-circuit current reached a maximum when the additive Au-NP volume was 0.50 mL, at

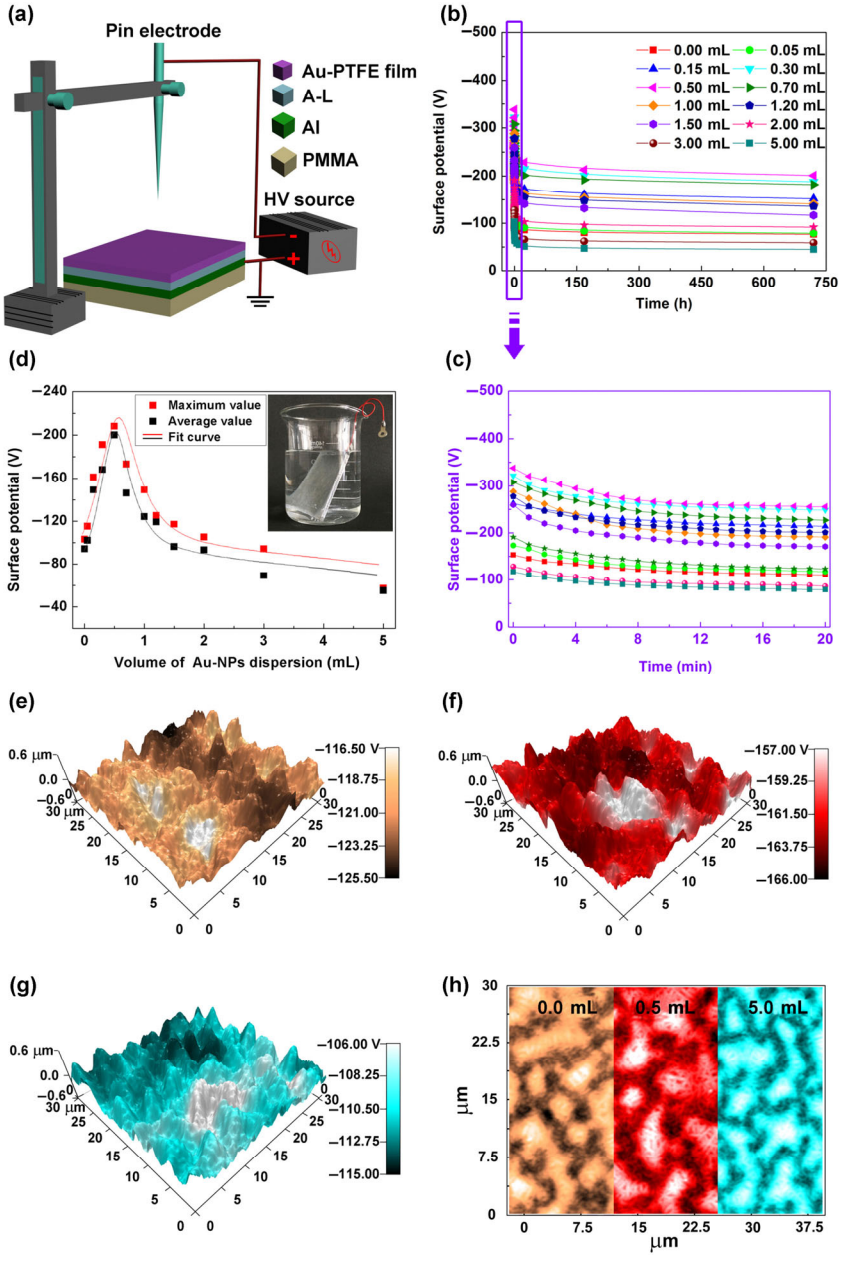

Figure 2 The experimental apparatus and results of negative high-voltage corona charging on the Au-PTFE nanocomposite films. (a) The device used for the corona charging. (b) Surface potential decay curves obtained for the Au-PTFE nanocomposite film (4 cm × 4 cm × 5 μm) exposed to normal air within 720 h at different volumes of Au-NP dispersion, (c) within 20 min magnified view, and (d) washed in water for 5 min (polarization time was 5 min, corona charging voltage –5 kV, vertical distance is 5 cm between the pin electrode and the Au-PTFE nanocomposite film). (e) Observed 3D surface potential of Au-PTFE nanocomposite films without Au-NP dispersion by AFM, (f) 0.5 mL 700 ppm Au-NP dispersion and (g) 5.0 mL 700 ppm Au-NP dispersion. (h) Surface morphology of Au-PTFE nanocomposite films are obtained by AFM.

233 V and 51 μA, respectively (Figs. 3(c) and 3(d)). Nevertheless, they began to gradually decrease when the Au-NP volume added was larger than 0.50 mL. Similarly, the transferred charge quantity and ESCD showed the same trend with maximum values of 135 nC and 85 μC/m², respectively, as shown in Figs. 3(e) and 3(f). In addition, the output performance of the TENG with an Au-PTFE nanocomposite film (0.50 mL Au-NPs) was 1.7 times larger with the pure PTFE film, indicating that the addition of an adequate quantity

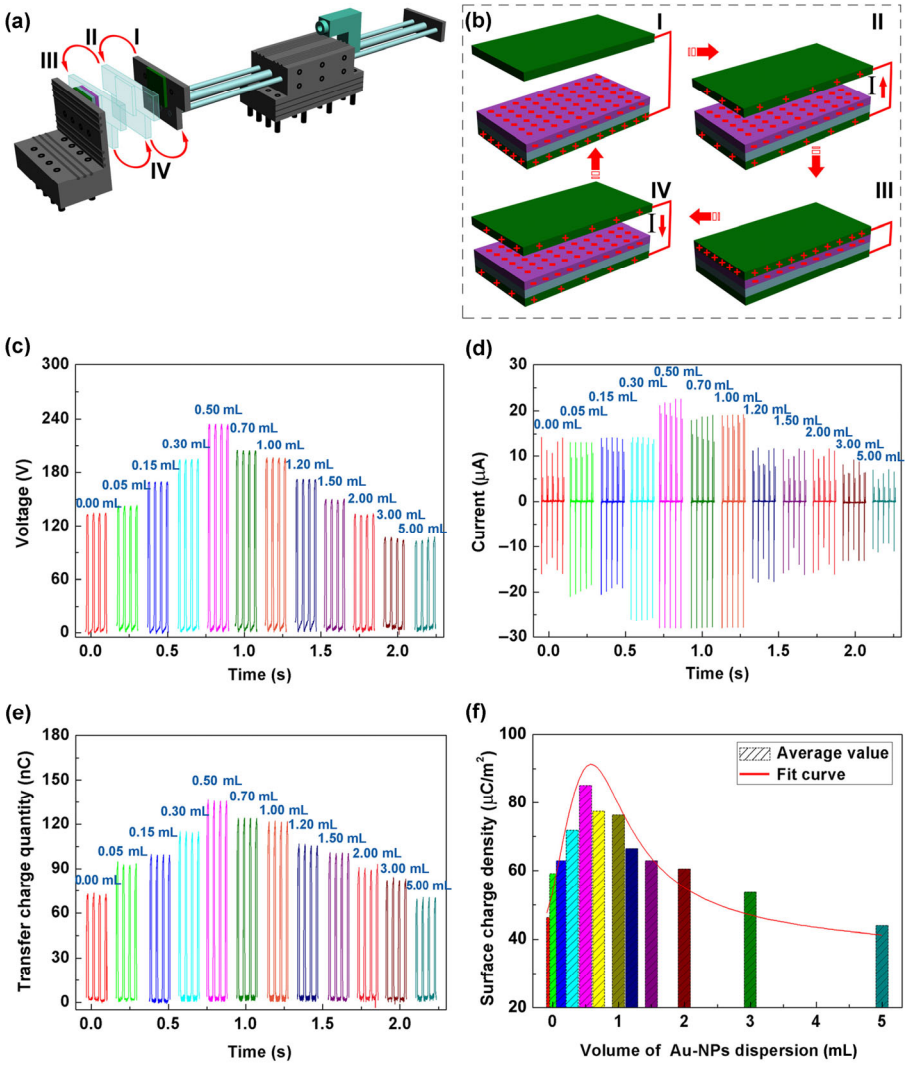

Figure 3 Operating principle of the contact-separation mode TENG built using the Au-PTFE nanocomposite films after corona charging. (a) Sketch of the TENG four steps working process. (b) Structure and electricity generation principle of the TENG. (c)–(e) The open-circuit voltage, short-circuit current, and transferred charges of the TENG measured based on different volume of Au-NPs, respectively. (f) The histogram of the ESCD on nanocomposite films under different volumes of Au-NPs.

of Au-NPs has a positive effect on the TENG's output.

Furthermore, the stability and durability of the Au-PTFE nanocomposite films after washing in water were tested with the additive Au-NP volume of 0.50 mL (Fig. 4). The output performance of the TENG does not significantly decline after being washed in water. The voltage, current and transferred charge quantity are plotted in Figs. 4(a)–4(c). Moreover, the durability of the TENGs with the nanocomposite films was measured after being washed, as shown in Figs. 4(d)–4(f), showing good tolerance to water. Figure 4(g) compares the output performance of the TENG with the pure PTFE and Au-PTFE film after being washed. It can be seen that the pure PTFE becomes dim, whereas the Au-PTFE TENG remains bright even after being washed. These results indicate that the stability and durability of the TENG based on the Au-PTFE nanocomposite film (0.50 mL Au-NPs) is superior.

Since PTFE is a nonpolar molecule (Figs. 5(a1) and 5(a2)), there is no dipole contained within (Fig. 5(b1)). When an external electric potential is applied, –5 kV in our experiments, the PTFE molecule will be polarized (Figs. 5(b2) and 5(b3)). The whole PTFE film will form a stable charge distribution lasting for a considerable amount of time, as shown in Fig. 5(b4). When Au-NPs

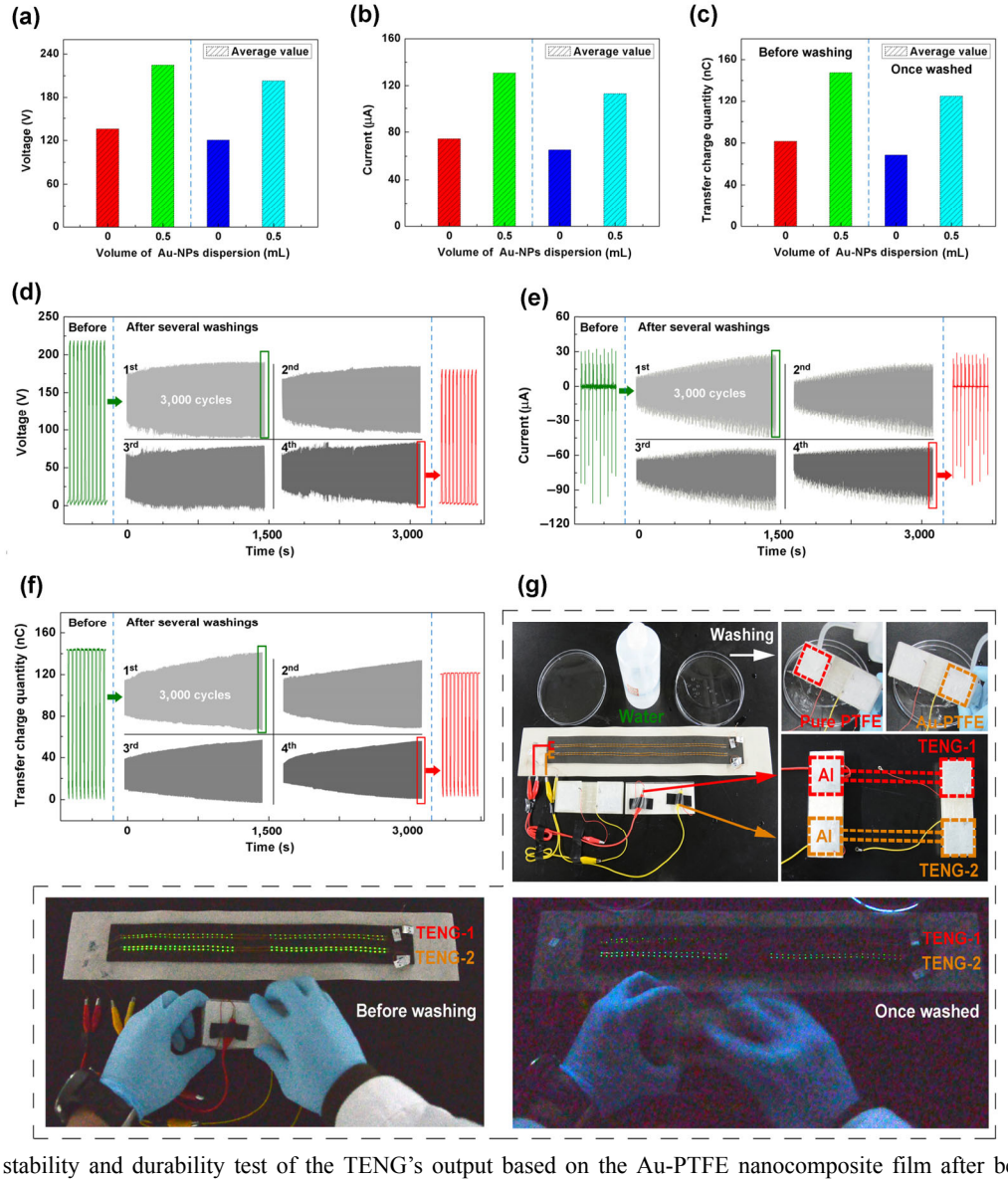

Figure 4 The stability and durability test of the TENG's output based on the Au-PTFE nanocomposite film after being washed in water. (a)–(c) Open-circuit voltage, short-circuit current, and transferred charges of the TENG measured before and after washing, with pure-PTFE and 0.5 mL Au-PTFE nanocomposite film, respectively. (d)–(f) The stability and durability test of the TENG's output for 3,000 cycles by water washing 4 times. (g) Digital photographs of 80 series connected green LEDs lit by the TENGs, of which TENG-1 was based on the pure PTFE film and the TENG-2 was based on the Au-PTFE nanocomposite film.

are added, during the corona charging, the Au-NPs are placed under two electric fields, the external field, E_0, (Fig. 5(c)) and the built-in field, E_1, from the polarized PTFE molecules (Fig. 5(d)). Consequently, an electric field around the Au-NPs is formed, as shown in Fig. 5(e2). These complex electric fields and nanoscale interfaces [35, 36] within the PTFE film are speculated to increase the film's capacity for trapping space charges [37–39], facilitating the achievement of a high ESCD (Figs. 5(e3) and 5(e4)). In addition, Au-NPs are distributed inside the PTFE, as shown in Fig. 6(a1). Every pair of particles with PTFE molecules in between them form a nanocapacitor (Figs. 6(b1)–6(c1)). We can simplify this model into multilayers of nanocapacitors serially connected from top to bottom (Figs. 6(a2)–6(c2)). A three-dimensional view of this set up was plotted in Figs. 6(a3)–6(c3). Assuming the Au-PTFE nanocomposite film thickness is d, the

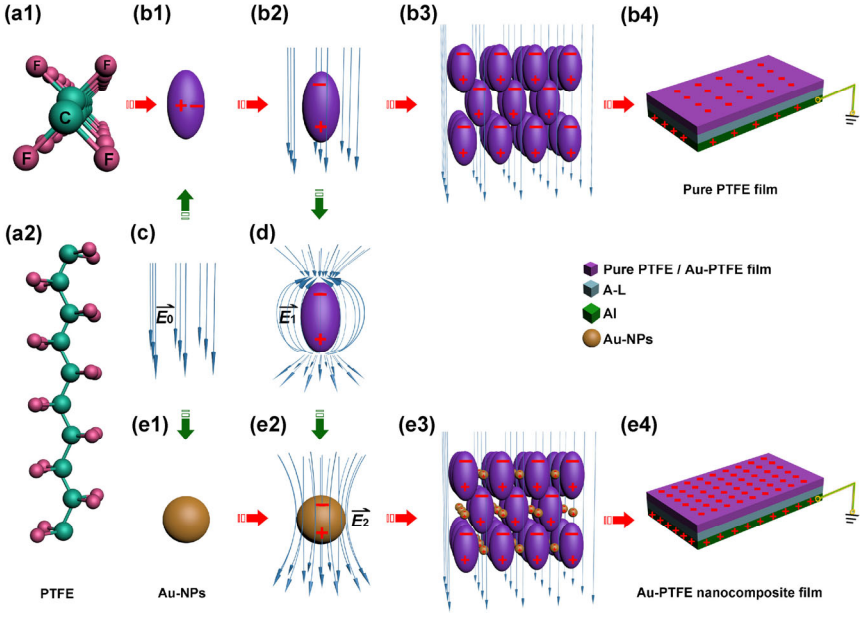

Figure 5 Charge injection principle of the Au-PTFE nanocomposite film by corona charging. E_0 is the electric field of corona charging, E_1 is the built-in field from the polarized PTFE molecules, E_2 is the electric field of the Au-NPs under the action of E_0 and E_1.

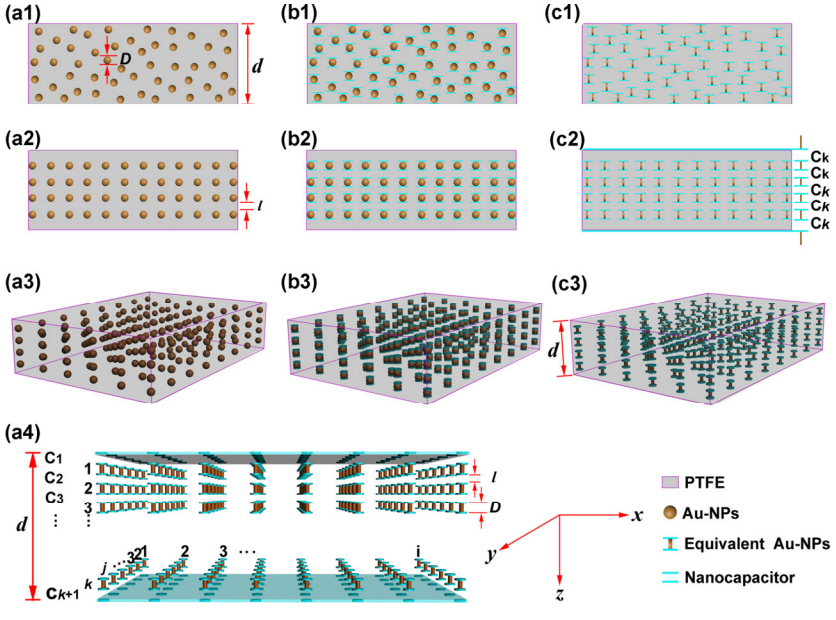

Figure 6 Schematic diagram of the nanocapacitor structures in the PTFE film. (a1) The distribution characteristics of the nanocapacitor structures, where the film thickness is *d*, and diameter of Au-NPs is *D*, (b1) same area as the electrodes, (c1) equivalent nanocapacitor, (a2)–(c2) the two-dimensional simplified model, with the layer spacing of *l*, (a3)–(c3) three-dimensional view, and (a4) the calculated section view of the equivalent nanocapacitor structures.

diameter of Au-NPs is *D*, the distance between the two NPs is *l*, and the numbers of the nanocapacitors along the *x*, *y* and *z* axes, are *i*, *j* and *k*, respectively (Fig. 6(a4)). According to the model of plane-parallel capacitors, we can calculate the composite film's capacitance as from Eq. (1)

$$C_c = \frac{\varepsilon_0 \varepsilon_1 S}{d} + \varepsilon_0 \varepsilon_1 ij\pi \left(\frac{D}{2}\right)^2 \left(\frac{1}{d-kD} - \frac{1}{d}\right) \quad (1)$$

Where ε_0, ε_1 and S are vacuum permittivity, relative

permittivity and the whole film's area (electrode surface), respectively. The first part is the sum of serial capacitances along the z axis within the area of the Au-NP, and the second part is the capacitance of the areas without Au-NPs along the z axis. As a comparison, the pure-PTFE film's capacitance can be expressed as

$$C_o = \frac{\varepsilon_0 \varepsilon_1 S}{d} \quad (2)$$

And subsequently

$$(k+1)l < d \quad (3)$$

Thus, it is clear that the composite film possesses larger capacitance. Therefore, under the same applied electric voltage, the composite film is likely to be able to store more charge [40]. However, with increasing concentration of Au-NPs, the average distance between two Au-NPs will decrease, leading to a higher electric field intensity and the possibility of breakdown of the local PTFE. Therefore, the film's charge density will decrease, which matches the results presented here (Figs. 2 and 3).

4 Conclusions

In summary, we designed nanocapacitor-embedded-structure films for use as an electret by filling PTFE with Au-NPs. It was demonstrated that the output current increased by a factor of 1.7 and with an ESCD of 85 μC/m². Simultaneously, we explored the relationship between maximum ESCD and the volume of added Au-NPs and its related theory. It was possible to achieve high output electricity from TENGs by adjusting the volume of added Au-NPs. Moreover, this nanocomposite film possesses excellent stability and durability. This work not only describes a new strategy to enhance the output of TENGs, but also contributes to the development of the material science and the fundamental understanding of the charge injection principle.

Acknowledgements

Thanks for the support from National Natural Science Foundation of China (Nos. 61405131, 51432005, 5151101243, and 51561145021), the National Key R&D Project from Minister of Science and Technology (No. 2016YFA0202704), Beijing Municipal Science & Technology Commission (No. Y3993113DF), and the "thousands talents" program for pioneer researcher and his innovation team, China.

Electronic Supplementary Material: Supplementary material (Video S1 demonstrates the stability and durability test of the TENG' output based on the Au-PTFE nanocomposite film being washed in water, Video S2 demonstrates the LEDs lighted up by TENG before washing, Video S3 demonstrates washing process and Video S4 demonstrates the LEDs lighted up by TENG after once washed) is available in the online version of this article at https://doi.org/10.1007/s12274-017-1716-y.

References

[1] Fan, F. R.; Tian, Z. Q.; Wang, Z. L. Flexible triboelectric generator. *Nano Energy* **2012**, *1*, 328–334.

[2] Wang, Z. L. Triboelectric nanogenerators as new energy technology for self-powered systems and as active mechanical and chemical sensors. *ACS Nano* **2013**, *7*, 9533–9557.

[3] Yang, W. Q.; Chen, J.; Zhu, G.; Yang, J.; Bai, P.; Su, Y. J.; Jing, Q. S.; Cao, X.; Wang, Z. L. Harvesting energy from the natural vibration of human walking. *ACS Nano* **2013**, *7*, 11317–11324.

[4] Zi, Y. L.; Niu, S. M.; Wang, J.; Wen, Z.; Tang, W.; Wang, Z. L. Standards and figure-of-merits for quantifying the performance of triboelectric nanogenerators. *Nat. Commun.* **2015**, *6*, 8376.

[5] Wang, Z. L. On Maxwell's displacement current for energy and sensors: The origin of nanogenerators. *Mater. Today* **2017**, *20*, 74–82.

[6] Zhang, Q.; Liang, Q. J.; Liao, Q. L.; Yi, F.; Zheng, X.; Ma, M. Y.; Gao, F. F.; Zhang, Y. Service behavior of multifunctional triboelectric nanogenerators. *Adv. Mater.* **2016**, *29*, 1606703.

[7] Zhang, Y.; Yang, Y.; Gu, Y. S.; Yan, X. Q.; Liao, Q. L.; Li, P. F.; Zhang, Z.; Wang, Z. Z. Performance and service behavior in 1-D nanostructured energy conversion devices. *Nano Energy* **2015**, *14*, 30–48.

[8] Wang, J.; Li, S. M.; Yi, F.; Zi, Y. L.; Lin, J.; Wang, X. F.; Xu, Y. L.; Wang, Z. L. Sustainably powering wearable

electronics solely by biomechanical energy. *Nat. Commun.* **2016**, *7*, 12744.

[9] Zhang, Y.; Yan, X. Q.; Yang, Y.; Huang, Y. H.; Liao, Q. L.; Qi, J. J. Scanning probe study on the piezotronic effect in ZnO nanomaterials and nanodevices. *Adv. Mater.* **2012**, *24*, 4647–4655.

[10] Yi, F.; Wang, X. F.; Niu, S. M.; Li, S. M.; Yin, Y. J.; Dai, K. R.; Zhang, G. J.; Lin, L.; Wen, Z.; Guo, H. Y. et al. A highly shape-adaptive, stretchable design based on conductive liquid for energy harvesting and self-powered biomechanical monitoring. *Sci. Adv.* **2016**, *2*, e1501624.

[11] Wang, X. F.; Niu, S. M.; Yin, Y. J.; Yi, F.; You, Z.; Wang, Z. L. Triboelectric nanogenerator based on fully enclosed rolling spherical structure for harvesting low-frequency water wave energy. *Adv. Energy Mater.* **2015**, *5*, 1501467.

[12] Wang, Z. L. Catch wave power in floating nets. *Nature* **2017**, *542*, 159–160.

[13] Chen, J.; Yang, J.; Li, Z. L.; Fan, X.; Zi, Y. L.; Jing, Q. S.; Guo, H. Y.; Wen, Z.; Pradel, K. C. Niu, S. M. et al. Networks of triboelectric nanogenerators for harvesting water wave energy: A potential approach toward blue energy. *ACS Nano* **2015**, *9*, 3324–3331.

[14] Xi, Y.; Guo, H. Y.; Zi, Y. L.; Li, X. G.; Wang, J. Deng, J. N.; Li, S. M.; Hu, C. G.; Cao, X.; Wang, Z. L. Multifunctional TENG for blue energy scavenging and self-powered wind-speed sensor. *Adv. Energy Mater.* **2017**, *7*, 1602397.

[15] Zhang, C.; Tang, W.; Han, C. B.; Fan, F. R.; Wang, Z. L. Theoretical comparison, equivalent transformation, and conjunction operations of electromagnetic induction generator and triboelectric nanogenerator for harvesting mechanical energy. *Adv. Mater.* **2014**, *26*, 3580–3591.

[16] Chen, J.; Huang, Y.; Zhang, N. N.; Zou, H. Y.; Liu, R. Y.; Tao, C. Y.; Fan, X.; Wang, Z. L. Micro-cable structured textile for simultaneously harvesting solar and mechanical energy. *Nat. Energy* **2016**, *1*, 16138.

[17] Tang, W.; Jiang, T.; Fan, F. R.; Yu, A. F.; Zhang, C.; Cao, X.; Wang, Z. L. Liquid-metal electrode for high-performance triboelectric nanogenerator at an instantaneous energy conversion efficiency of 70.6%. *Adv. Funct. Mater.* **2015**, *25*, 3718–3725.

[18] Tang, W.; Meng, B.; Zhang, H. X. Investigation of power generation based on stacked triboelectric nanogenerator. *Nano Energy* **2013**, *2*, 1164–1171.

[19] Ha, M.; Park, J.; Lee, Y.; Ko, H. Triboelectric generators and sensors for self-powered wearable electronics. *ACS Nano* **2015**, *9*, 3421–3427.

[20] Wang, J.; Li, S. M.; Yi, F.; Zi, Y. L.; Lin, J.; Wang, X. F.; Xu, Y. L.; Wang, Z. L. Sustainably powering wearable electronics solely by biomechanical energy. *Nat. Commun.* **2016**, *7*, 12744.

[21] Han, C. B.; Zhang, C.; Li, X. H.; Zhang, L. M.; Zhou, T.; Hu, W. G.; Wang, Z. L. Self-powered velocity and trajectory tracking sensor array made of planar triboelectric nanogenerator pixels. *Nano Energy* **2014**, *9*, 325–333.

[22] Wang, Z. L.; Chen, J.; Lin, L. Progress in triboelectric nanogenerators as a new energy technology and self-powered sensors. *Energy Environ. Sci.* **2015**, *8*, 2250–2282.

[23] Wang, X.; Wang, S. H.; Yang, Y.; Wang, Z. L. Hybridized electromagnetic-triboelectric nanogenerator for scavenging air-flow energy to sustainably power temperature sensors. *ACS Nano* **2015**, *9*, 4553–4562.

[24] Chen, S. W.; Gao, C. Z.; Tang, W.; Zhu, H. R.; Han, Y.; Jiang, Q. W.; Li, T. Cao, X.; Wang, Z. L. Self-powered cleaning of air pollution by wind driven triboelectric nanogenerator. *Nano Energy* **2015**, *14*, 217–225.

[25] Sakane, Y.; Suzuki, Y.; Kasagi, N. The development of a high-performance perfluorinated polymer electret and its application to micro power generation. *J. Micromech. Microeng.* **2008**, *18*, 104011.

[26] Yu, Z. Z.; Watson, P. K.; Facci, J. S. The contact charging of PTFE by mercury: The effect of a thiophene monolayer on charge exchange. *J. Phys. D Appl. Phys.* **1990**, *23*, 1207–1211.

[27] Wei, X. Y.; Zhu, G.; Wang, Z. L. Surface-charge engineering for high-performance triboelectric nanogenerator based on identical electrification materials. *Nano Energy* **2014**, *10*, 83–89.

[28] Wang, S. H.; Xie, Y. N.; Niu, S. M.; Lin, L.; Liu, C.; Zhou, Y. S.; Wang, Z. L. Maximum surface charge density for triboelectric nanogenerators achieved by ionized-air injection: Methodology and theoretical understanding. *Adv. Mater.* **2014**, *26*, 6720–6728.

[29] Zhu, G.; Lin, Z. H.; Jing, Q. S.; Bai, P.; Pan, C. F.; Yang, Y.; Zhou, Y. S.; Wang, Z. L. Toward large-scale energy harvesting by a nanoparticle-enhanced triboelectric nanogenerator. *Nano Lett.* **2013**, *13*, 847–853.

[30] Cheng, G.; Zheng, L.; Lin, Z. H.; Yang, J.; Du, Z. L.; Wang, Z. L. Multilayered-electrode-based triboelectric nanogenerators with managed output voltage and multifold enhanced charge transport. *Adv. Energy Mater.* **2015**, *5*, 1401452.

[31] Lin, Z. H.; Cheng, G.; Lee, S.; Pradel, K. C. Wang, Z. L. Harvesting water drop energy by a sequential contact-electrification and electrostatic-induction process. *Adv. Mater.* **2014**, *26*, 4690–4696.

[32] Wu, Y. C.; Zhong, X. D.; Wang, X.; Yang, Y.; Wang, Z. L. Hybrid energy cell for simultaneously harvesting wind, solar, and chemical energies. *Nano Res*. **2014**, *7*, 1631–1639.

[33] Paajanen, M.; Wegener, M.; Gerhard-Multhaupt, R. Understanding the role of the gas in the voids during corona charging of cellular electret films—A way to enhance their piezoelectricity. *J. Phys. D Appl. Phys*. **2001**, *34*, 2482–2488.

[34] Zhou, T.; Zhang, L. M.; Xue, F.; Tang, W.; Zhang, C.; Wang, Z. L. Multilayered electret films based triboelectric nanogenerator. *Nano Res*. **2016**, *9*, 1442–1451.

[35] Doyle, W. T.; Jacobs, I. S. Effective cluster model of dielectric enhancement in metal-insulator composites. *Phys. Rev. B Condens. Matter* **1990**, *42*, 9319–9327.

[36] Doyle, W. T.; Jacobs, I. S. The influence of particle shape on dielectric enhancement in metal-insulator composites. *J. Appl. Phys*. **1992**, *71*, 3926–3936.

[37] Sessler, G. M.; West, J. E. Studies of electret charges produced on polymer films by electron bombardment. *J. Polym. Sci. Part B Polym. Lett*. **1969**, *7*, 367–370.

[38] Liu, C. Y.; Bard, A. J. Electrons on dielectrics and contact electrification. *Chem. Phys. Lett*. **2009**, *480*, 145–156.

[39] Yu, Z. Z.; Watson, P. K. Contact charge accumulation and reversal on polystyrene and PTFE films upon repeated contacts with mercury. *J. Phys. D Appl. Phys*. **1989**, *22*, 798–801.

[40] Yu, Z. Z.; Watson, K. Two-step model for contact charge accumulation. *J. Electrostat*. **2001**, *51–52*, 313–318.